Title: $TiAg_x$ thin films for lower limb prosthesis pressure sensors: effect of composition and structural changes on the electrical and thermal response of the films

Author: C. Lopes C. Gonçalves P. Pedrosa F. Macedo E. Alves N.P. Barradas N. Martin C. Fonseca F. Vaz

PII: S0169-4332(13)01329-9
DOI: http://dx.doi.org/doi:10.1016/j.apsusc.2013.07.021
Reference: APSUSC 25995

To appear in: *APSUSC*

Received date: 3-4-2013
Revised date: 4-7-2013
Accepted date: 6-7-2013

Please cite this article as: C. Lopes, C. Gonçalves, P. Pedrosa, F. Macedo, E. Alves, N.P. Barradas, N. Martin, C. Fonseca, F. Vaz, $TiAg_x$ thin films for lower limb prosthesis pressure sensors: effect of composition and structural changes on the electrical and thermal response of the films, *Applied Surface Science* (2013), http://dx.doi.org/10.1016/j.apsusc.2013.07.021

$TiAg_x$ thin films for lower limb prosthesis pressure sensors: effect of composition and structural changes on the electrical and thermal response of the films

C. Lopes[1], C. Gonçalves[1], P. Pedrosa[1,2,3], F. Macedo[1], E. Alves[4], N.P. Barradas[5], N. Martin[6], C. Fonseca[2,3], F. Vaz[1*]

[1]Centro de Física, Universidade do Minho, 4710-057 Braga, Portugal

[2]Universidade do Porto, Faculdade de Engenharia, Departamento de Engenharia Metalúrgica e de Materiais, Rua Roberto Frias, s/n, 4200-465 Porto, Portugal

[3]SEG-CEMUC – Departamento de Engenharia Mecãnica, Universidade de Coimbra, 3030-788 Coimbra, Portugal

[4]Associação Euratom/IST, Instituto de Plasmas e Fusão Nuclear, Instituto Superior Técnico, Universidade Técnica de Lisboa, Av. Rovisco Pais, 1049-001, Lisboa, Portugal

[5]Campus Tecnológico e Nuclear, Instituto Superior Técnico, Universidade Técnica de Lisboa, E.N. 10, 2686-953 Sacavém, Portugal

[6]Institut FEMTO-ST, UMR 6174, Université de Franche-Comté, CNRS, ENSMM, UTBM, 32, Avenue de l'observatoire, 25044 BESANCON Cedex, France

ABSTRACT

Titanium-silver, Ti-Ag, thin films display excellent biocompatibility and reveal great potential to be used as conductive materials for prosthesis pressure sensors. In the frame of this work, $TiAg_x$ thin films were deposited onto silicon and glass substrates by DC magnetron sputtering, using a pure Ti target containing different amounts of Ag pellets. The films display Ag/Ti ratios varying from 0 up to 0.36, resulting in relatively large range of composition,

*To whom all correspondence should be sent (fvaz@fisica.uminho.pt)

which gave rise to varied morphological, structural and some selected property responses. For Ag/Ti ratios below 3.0×10^{-3}, the $TiAg_x$ films exhibited similar behaviour to those of standard Ti films. Above this critical value, the role of Ag becomes crucial on the crystallographic structure evolution, as well as on the surface morphology changes of the films. A gradual increase of the Ag/Ti ratio lead to the growth of Ti-Ag crystalline phases, whereas the long range order of Ti grains was reduced from 22 nm down to 7 nm. Similarly, a denser microstructure was developed with a reduction of the sharpness of the surface morphology. This critical Ag/Ti ratio ($<3.0\times10^{-3}$) also corresponded to an enhanced electrical resistivity, which reached a value of ρ_{300K} = 72 μΩ cm. The thermal characterization revealed a similar trend, with the existence of two clear distinct zones, related again with the different critical composition ratios and the correspondent changes in both morphology and structural features.

Keywords: Pressure sensors; TiAg films; XRD; electrical resistivity; thermal conductivity.

1. INTRODUCTION

There are several types of trauma or diseases that could culminate in limb amputation. After the amputation, the limb is partially or completely replaced by prosthetic devices, which according to the EU Directive (42/93/EC) are custom-made medical devices. They are intended to compensate impairments and mobility limitations, allowing a similar counter lateral, comfortable and safe gait to the amputee. There are frequently inadequacies, consisting often on non-adequate fit of the prosthesis and thus poor static and dynamic weight support, gait deviations and non-efficient gait. As a consequence, in most cases, there is an overload of the non-amputated side and high-energy consumption, which, in extreme situations, leads to the stopping of use of the device by the amputee. The production of the prosthesis, and its fit to the amputees, implies alignment of the socket and structure, referring

to defined parameters. These assessments are done using qualitative methods, which are based on the experience of the physiatrist and therefore not reproducible and not always reliable [1-4].

Starting with this need of having quantitative and reliable information on the suitability of a given prosthesis, different approaches have been carried out to monitor the strain or pressure fields that are developed all over the contact surface between the patient and the prosthesis. Knowledge of these pressure maps can lead to further optimization of the prosthesis, both in terms of the shape and the alignment of the socket, contribution in a single way to increase patient's comfort. The present work is a one-step towards the development of a sensor network device, designed to monitor the pressure fields at the prosthesis/limb interface, especially in artificial lower limbs. The idealization of such a sensor network device relies on some basic criteria, including: i) the need to have a linear response with applied pressure (high sensibility to the pressure); ii) the importance to have low sensitivity to temperature, material composition and manufacturing technique; and, in addition, iii) no phase transitions should be found at the operation temperature [5]. Therefore and given its desired properties (resistance, high flexibility, low density, lightweight, low mechanical impedance) [6, 7], the proposed sensor array is being developed and implemented from poli(vinylidene fluoride)-PVDF. This material has remarkable piezoelectric (sensitive to dynamic pressure fields) and piezoresistive (measure static and dynamic deformations) properties [8], that should provide a good response for both low and high magnitude mechanical pressures that are expected to arise in the limb prosthesis when used by the amputee [5, 8-13].

Beyond the specific nature and characteristics of the chosen base smart polymeric sensing material (PVDF), there is still the need for its surface functionalization, namely in terms of electric contact. The present approach consists in using a magnetron sputtered conductive thin

layer to detect, amplify and linearize the strain-induced electric charge or the current, produced by the reversible mechanical deformation in the polymeric substrate.

Taking into account the main requirements of the targeted application, the selected layer system should reveal high corrosion and wear resistance, high conductivity and high elasticity (deformation resistance) and, additionally, a good chemical, thermal and mechanical stability. For most metallic materials, the resistance changes as a function of the strain are linear and for this reason, they are convenient for pressure and force sensors [14]. Furthermore, coated polymers will be subjected to mechanical and electrical solicitations and physical contact with the human stump that can cause degradation of the coating, and therefore can affect its functional performance. Given the features of the individual elements, the Ti-Ag system was selected. The use of Ti relies on its biocompatibility with human tissues, corrosion resistance, strength, elasticity and excellent thermal and chemical stability [15, 16]. Likewise, and as it is well-known, Ag exhibits a high electrical conductivity, it is quite soft and ductile and it is a powerful antibacterial material. When implanted on a material surface, it can exhibit well-effective antibacterial characteristics, preventing the formation of bacteria biofilm that could cause inflammation and infection [17-20]. These are crucial parameters within any prosthesis to be used by humans. Thus, the addition of Ag was planned in order to tailor the films' flexibility and electrical response, aiming at the same time to give an extra input in terms of biocompatibility due to its bactericide effect.

Taking all this into account, the purpose of the present paper is to give a first insight on the influence of Ag additions on the structural and morphological changes of Ti-Ag nanocomposite thin films, and their influence in one of the most important properties of the targeted application - electrical response, as well as in a crucial property for the patient's comfort – the material thermal characteristics, which may influence not only the adequacy of the pressure sensors in their main target, but also the reliability of the device itself.

2. EXPERIMENTAL DETAILS

$TiAg_x$ thin films were deposited onto glass and single crystal (100) silicon substrates (2×2 cm^2 in dimension), by reactive DC magnetron sputtering. The depositions were carried out in a pure argon atmosphere, in a custom-made deposition system. The substrates were ultrasonically cleaned in ethanol 96% (vol.) before introducing them into the reactor. The films were prepared with the substrate holder positioned at 70 mm from the target, using a DC current density of 100 $A.m^{-2}$ on the Ti target (200×100×6 mm^3, 99.96 at.% purity). Different amounts of Ag pellets were placed in the preferential erosion zone of the Ti target in order to change the Ag concentration in the coatings. The total area occupied by the Ag pellets ranged from 0.13 cm^2 to 8.3 cm^2. The base pressure was always below $2.0x10^{-4}$ Pa, and the Ar pressure was kept constant at 0.3 Pa during deposition. The coatings were grown in rotation mode (7 rpm), without applying any bias voltage (grounded condition). The deposition temperature was set to 100 ºC. All these requirements (no bias and low deposition temperature) were selected in order to optimize the n film system according to the basic requirements of the targeted pressure sensor material –PVDF). Taking this into account, the discharge parameters (target potential, pressure and temperatutre) were monitored during the deposition, using a Data Acquisition/Switch Unit Agilent 34970A, with a multifunction module (334907A. This unit uses a RS-232 interface, and the data was acquired with a Benchlink Data Logger III software.

The deposition rate was calculated from the ratio between the average thickness (calculated from five measurements in each sample) of the samples and the deposition time (1 h for all coatings). Scanning electron microscopy (SEM), was used to determine the thickness of the films and to probe their morphological features, using a FEI Quanta 400FEG ESEM operating at 15 keV. The atomic composition of the as-deposited samples was measured by

Rutherford Backscattering Spectroscopy (RBS), using a 1.9 or 2 MeV ^{4}He beam, at normal incidence. Three detectors were used, one located at 140º, and two pin-diode detectors located symmetrical each other, both at 165º. Composition profiles for the as-deposited samples were determined using the software NDF [21], after three different measurements in each sample and the analysed area was about 0.5×0.5 mm^2. The error in the Ag concentrations is around 0.02 at.% for concentrations below around 0.1 at.%, where the statistical error dominates the total uncertainty. The error increases to around 0.5 at.% for higher Ag concentrations (above around 10 at.%), where systematic effects are more important. The structure and phase distribution of the coatings was accessed by X-ray diffraction (XRD), using a conventional Philips PW 1710 diffractometer, operating with Cu K_α radiation, in a Bragg-Brentano configuration. The XRD patterns were deconvoluted and fitted with a Voigt function to determine the structural characteristics of the films, such as the peak position (2θ) and the full width at half maximum (FWHM).

The coatings reflectivity was measured on glass substrates between 250 and 2500 nm using a Shimadzu UV-3101 PC UV–vis–NIR, with an attached integrating sphere of 60 mm (inner diameter). With the purpose of eliminating experimental artefacts caused by the integrating sphere, two standards, a STAN-SSH High- Reflectivity Specular Reflectance Standard (from Ocean Optics) and a WS-1-SL Spectralon White Reflectance Standard (from Labsphere), were used for reflectance measurement correction purposes. This optical characterization was carried out with the main purpose to get further insights on the particular state of silver in the coatings, namely its possible bonding states.

The films electrical resistivity was measured using the four-probe van der Pauw method [22]. Infra Red Radiometry measurements were performed in order to get information on the thermal properties of the $TiAg_x$ thin film samples. To create the small thermal oscillations in the samples, an intensity modulated laser beam was the usual excitation source. Detection was

made with a HdCdTe IR detector (2-12 μm) connected to a lock-in amplifier (SR830). Extensive details on the experimental conditions and setup can be found in references [23-25].

3. RESULTS AND DISCUSSION

3.1. Discharge characteristics: target potential and deposition rate

Figure 1 shows the evolution of both target potential and deposition rate as a function of the area of the Ag pellets, placed on the target erosion zone. According to the evolution of the target potential during the depositions (Fig. 1a), two different zones can be identified. In the first one – Zone I, relatively small areas of Ag were exposed and the target potential presented a tenuous decrease. Voltage values decrease from 332 V to 322 V (roughly 3%), close to the value of the Ti reference thin film. For the second zone - Zone II, the area of exposed Ag becomes significant (higher than 1 cm^2) compared to the target area (200 cm^2), which resulted in an almost linear increase of the target potential, varying from about 319 V to approximately 357 V (about 12% increase). In order to understand such a two-fold evolution, one must keep in mind that magnetron sputtering is a complex process, depending on several parameters that are strongly correlated. These include the target condition, the magnetron configuration, target power and the discharge gases. For the present work, and given the similar deposition parameters that were selected, the target potential seems to be largely influenced by the composition of the target itself and by the processes that are occurring during sputtering, which reveals a strong influence of the plasma characteristics [26, 27].

The discharge voltage measured during magnetron sputtering, at constant current and sputtering pressure (as in this work), is inversely proportional to the ion induced secondary electron emission (ISEE) coefficient of the target material [28], in agreement with equation (1) proposed by Thornton [27]:

$$V_{min} = \frac{W_0}{\gamma_{ISEE} E \varepsilon_i \varepsilon_e} \quad (1)$$

where W_0 stands for the effective ionisation energy (about 30 eV for Ar^+) [29], ε_i stands for the ion collection efficiency and ε_e for the fraction of the maximum number of ions (for magnetron sputtering ε_i and ε_e are close to unity). E represents the effective gas ionization probability and γ_{ISEE} for the ion induced secondary electron emission coefficient. Based on the empirical relations and measured values for the γ_{ISEE} coefficient; Depla et al. [26, 27] determined an averaged value for several materials. In the case of the present study, the Ag coefficient is lower than that of Ti (γ_{ISEE} (Ag) = 0.110 and γ_{ISEE} (Ti) = 0.114). Thus, an increase of the number of Ag pellets leads to a lower exposed area of Ti, which is expected to result in higher values of the target potential since it is inversely proportional to the γ_{ISEE} of the target material. This may explain the behaviour observed for the films prepared within Zone II, where the increase of the exposed Ag plays the major role in the composition of the target. In the case of Zone I, the addition of a small number of Ag pellets on the Ti target surface may act essentially as if it was a titanium impurity, rather than a change in the target composition itself. In this way, only small changes in the target potential are expected, as is in fact observed.

Fig. 1b shows the evolution of the deposition rate as a function of the Ag exposed area, showing a gradual decrease of this characteristic with the increase of the Ag amount in the target. Again, a closer look reveals that the films prepared with Ag exposed areas below 1.3 cm^2, Zone I, the deposition rate varies only slightly between 1.6 μm/h and 1.7 μm/h, comparing with a slight variation that was also observed for the target potential evolution. In contrast, the $TiAg_x$ thin films prepared with higher amounts of Ag pellets in the target (Ag exposed areas above 1.3 cm^2, Zone II), present a clear tendency for a more pronounced decrease of the deposition rate, also associated with the previous variation of the target potential, which presented an abrupt increase within this same zone.

In terms of the basic mechanisms that may explain this kind of behaviour, one must keep in mind that the sputtering of atoms from an elemental target is approximately uniform. However, the sputtering of multicomponent targets depends significantly on the sputtering yields of each atomic species, their different masses and their interactions as a compound. The main effect in the sputtering of multicomponent targets is that the different components are generally in different phases and often exhibit different crystal structures. Then, they are not ejected in proportion to their area on the target surface. This effect is called preferential sputtering and was discussed by several authors [27, 28, 30-32]. Bibic et al. [31] concluded that sputtering yield of Ag in a AgCu alloy decreases considerably compared to a single silver phase, while Pierson et al. [32] reported a "shadowing effect" during the deposition. For these authors, the sputtering yield decreases due to the development of the roughened surface topography. These authors claimed that, in the presence of roughness, the sputtered flux is partially directed towards other nearby features leading to re-deposition of material, decreasing the mass loss and lowering the effective sputtering yields. All these observations are in agreement with the gradual decrease of deposition rate, where the high known value of Ag sputtering yield is minimized by the composed target effect.

3.2. Composition of the as-deposited samples

Figure 2 shows the chemical composition of the prepared coatings, obtained by RBS spectra analysis, as a function of the Ag exposed area on the target surface. The existence of the two distinct groups of samples is well correlated with the two zones previously suggested. In the first group (Zone I), Ti is the main component, with an atomic percentage close to 99 at.% - a Ti-rich zone. For the second group (Zone II), the amount of Ag pellets placed on the target was significantly increased (Ag exposed area in the preferential eroded zone increases from 1.3 cm^2 to 8.3 cm^2) and consequently its content in the films also increased, from 5.6

at.% to 26.5 at%, while Ti content decreased from 94.4 at.% to 73.5 at.%. Since Ti and Ag atomic concentrations display an opposite trend, the Ag/Ti ratio will be used hereafter to label the samples and to discuss how the changes observed in structural and morphological characterization may affect the functional properties of the samples.

Important to note is that this variations in the elemental composition ratios of the films is expected to give rise to a wide range of film responses, namely those related with the targeted application: a thin film system for lower limb prosthesis pressure sensors. As previously mentioned, one of such important responses is the electrical one. The tailoring of the film's resistivity will certainly dependent much on the particular compositional ratio of the films, and its influence on the specific morphology and structure, which will be optimized according to the particular requirements of such a pressure sensor. In this respect, the wide range of Ag additions will be of major importance to optimize the films mechanical responses, namely its elastic modulus, which will be crucial when exploring the possibility to deposit the present thin film system within flexible-like pressure sensors.

3.3. Structural and morphological characterization

The structural characterization carried out by XRD, Fig. 3, displays once again the two clear distinct zones. For Zone I, Ti was identified as the major component and the coatings are polycrystalline, exhibiting a typical hexagonal close packing (hcp) structure of Ti, with a preferential (002) growth orientation (ICSD database, card #181718). With the increase of the Ag/Ti ratio (above 3.0×10^{-2}), the preferential growth changes to (011). Moreover, XRD diffraction patterns (Fig. 3a) reveal a slight shift to higher angular positions, indicating possible lattice distortions due to smaller lattice parameters. This should result from some possible vacant positions of Ti in the hcp structure, probably because Ti atoms are establishing intermetallic bonds with the few Ag atoms that arrived on the growing film since

the standard enthalpies of formation of Ag-Ti compounds are favorable [33]. Furthermore, and since Ag and Ti atoms exhibit similar atomic radii [34], the substitution of Ti by Ag should not be disregarded [35]. At the same time, there is no clear evidence for the presence of a silver phase for this low Ag content zone. Anyway, one must keep in mind that the nonexistence of Ag peaks may not be a direct indication of a Ag phase absence, since it may exist in an amorphous state or its content is bellow the detection limit [36].

For Ag/Ti ratios above 1.2×10^{-1} (Zone II), additional diffraction patterns can be seen (2θ = 37.9, 44.1º and 64.2º) (Fig. 3a and 3b). Their indexing remains uncertain since they may correspond to different phases according to the ICSD database, namely a Ti_2Ag (card # 605935), a TiAg (card # 605934) or even a pure Ag phase (card # 181730). In fact, the angular positions are too close to allow an unequivocal identification. Therefore, this set of results only suggests that there may exist a Ti phase with one of the three Ag phases, or even a mixture of all or two of them [33, 37-39]. Anyway, with the increase of the silver content, the angular positions that are observed, compared to the diffraction pattern of the pure Ag film, seem to indicate that an fcc-Ag phase may prevail over the titanium or titanium silver phases (Fig. 3b).

On the other hand, with growing Ag additions it is noteworthy that the well-defined Ti crystal structure from Zone I becomes increasingly amorphous in Zone II, as demonstrated from the substantial increase of the full width at half maximum (FWHM). There can be several reasons for this progressive amorphization. First, it is possible that an increasing number of Ag atoms are incorporated in the hcp-Ti structure, as substitutional or interstitial atoms. In addition, the low adatom mobility due to relatively low deposition temperature (100 ºC), associated with the absence of ion bombardment (films were grown in ground condition) would certainly favor these Ag incorporations in the Ti lattice. This incorporation would lead to cumulative local lattice disorder, and thus to a progressive tendency to the amorphization

of the Ti phase [35].

The Ti-Ag phase diagram [33] shows that at low Ag concentrations, < 3 at.%, a solid solution of Ag in α-Ti is favored, while at higher Ag concentrations a binary phase mixture of α-Ti and Ti_2Ag, is thermodynamically more favorable, and might be present at the solid state [33, 40]. Although the equilibrium phase diagram suggests that for the Ag/Ti atomic ratios obtained in this work, the metallic Ag cannot precipitate, the unfavorable growth conditions in this work (no bias and relatively low deposition temperature) limited the adatom mobility on the growing film. This may give rise to local thermal spikes, leading to thermodynamic non-equilibrium conditions. These non-equilibrium conditions could explain the precipitation of metallic Ag particles, coexisting with TiAg and Ti_2Ag solid solutions [41]. This would induce a mixture of Ag phases, as the XRD patterns may reveal (Fig. 3a and 3b).

In order to get further insights on this possible silver phases mixture, UV–visible reflectance measurements were carried out, since they are a powerful method to detect the occurrence of metallic Ag nanograins [42], and thus uncover some possibilities already advanced. In fact, according to the work of Catrin et al. [42], metallic Ag exhibit a characteristic absorption band at 320 nm and reflectance values higher than 95% in the visible region [43], when deposited at room temperature. Figure 4 shows the reflectance measurements in the visible region for the set of $TiAg_x$ coatings. Contrarily to what could be expected, the results indicate that the Ag atoms are probably not segregated into a metallic phase, since no absorption band is clearly detected in the spectra. This may be a strong indication for the existence of any of the Ti-Ag phases previously mentioned, or even a mixture of both. This figure also shows an increase in the reflectance values with the increase of the Ag content, although not exceeding the limit of 50% in the visible region.

Besides a change in the structural features of the films with the increase of the Ag content, there is also a change in terms of the microstructure of $TiAg_x$ thin films, which again

will have an effect on the physical properties of the films. Figure 5 shows SEM plan view and cross-section images of representative films, denoting the effect of the increase of the Ag content on their microstructure. Beyond a relatively homogeneous thickness that one can esily observed for all deposited coatings, this figure shows that within Zone I films, the coatings displayed the typical Ti morphology structure [15], with the formation of three-dimensional hexagonal grain features at the surface (Fig. $5a_1$, b_1, c_1), and a characteristic columnar-like growth (Fig. $5a_2$, b_2 and c_2), which is expected given the low Ag content. It is also interesting to note that the Ag addition, even in small amounts, promotes some clear reduction of the surface roughness and maintains the columnar structure. With further increasing the Ag content (Ag/Ti ratio higher than 3.0×10^{-2} - Zone II), the characteristic hexagonal grain feature of Ti-rich thin films at the surface vanishes. The samples from this zone develop smoother surfaces, with fine and denser microstructures. For the samples with the highest Ag/Ti ratio (Fig. $5e_1$ and e_2), brighter spots can be identified at the surface, which are probably from TiAg clusters segregated from the Ti hexagonal grain boundaries.

3.4. Electrical and thermal characterization

The electrical resistivity of metallic systems is very sensitive to the particular electronic structure and its evolution, as well as to the set of morphological characteristics and their influence on the availability of charge carriers in the system. Charge carriers resistance is caused by the scattering of electrons due to disturbances in the crystal structure and morphology such as solute elements, impurities, grain boundaries, dislocations and vacancies [44]. The total resistivity, at a specific temperature, is the result of various scattering processes, that was simplified by Matthiessen's rule, where total resistivity is expressed by the sum of all the calculated terms [45]:

$$\rho_{\text{tot}} = \rho_0 + \rho_{ph} + \rho_{mag} \quad (2)$$

where the subscripts denote the residual resistivity (*0*), the resistivity owing to phonon scattering (*ph*) and the resistivity owing to spin-dependent scattering (magnetic scattering processes, *mag*) [45].

The effect of the variable ‘‘impurity’’ scattering is particularly evident for pseudo-binary systems, in agreement with the so-called Nordheim's rule [44, 45]. For this specific case, the dependence of residual resistivity (ρ_0), on a single solute is expressed as:

$$\rho_0(x) = Ax\,(1 - x) \quad (3)$$

where *x* is the concentration of the solute and A is a constant which depends on the base metal and solute. The value of A increases with differences in valence, atomic size or other quantities between the solvent and the solute.

In order to study the electrical properties of $TiAg_x$ system, electrical resistivity measurements at room temperature were carried out, and the obtained results (Fig. 6) confirm the evidence of two distinct electrical behaviours, as previously claimed in previous sub-chapters. Figure 6 shows that for low Ag contents (< 6 at.%), the resistivity values of the films are rather similar to those of bulk Ti (around 43 μΩ·cm) [46]. For the values obtained in this first zone (Zone I), and according to Nordheim’s rule, Ag atoms could play the role of solute impurities in the Ti solvent structure (as in fact already mentioned) and a resistivity increase, relatively to the Ti thin film, is expected due to the probability of the charge carriers being scattered by impurities. However, it is also commonly reported that grain size can have also an important role in the evolution of the electrical properties (namely resistivity) of a given thin film system. In order to uncover this possibility in the present system, Fig. 7 shows the evolution of the thin films grain size as a function of the Ag content. From this figure, it is worth noticing a sharp decrease of the grain size from 22 nm to 12 nm within the films from Zone I. This significant decrease of grain size would, in a first approximation, give rise to an

increase in the resistivity due to the increase of grain boundaries scattering. Anyway, the results obtained for the films within this first zone are somewhat contradictory since an approximately constant value of resistivity is observed for all samples. One of the reasons for this behaviour might be related to the good electrical conduction properties of Ag that simultaneously plays a dual role in the Ti structure: impurity and charge carrier, and thus "smoothening" the effect of the grain size reduction and the expected increase of resistivity that it usually induces.

In addition, a sudden increase of resistivity values can be noticed when going from Zone I to Zone II (from about 40 μΩ·cm to 70 μΩ·cm), which actually corresponds to a change of composition zone (Fig. 2), but above all, to the exact transition in terms of structural features displayed in Fig 3. The changes in the crystalline phases that are developed, together with the relatively low values of grain size in the films from Zone II (about 10 nm) in comparison to those of Zone I (above 12 nm), are certainly parameters that must account for this two-fold behavior. In Zone II, it is also important to note a general decrease of the electrical resistivity, which could result from the improved crystallinity of the coatings revealed by a larger crystallite size of the silver phases (Fig. 7). All these changes in the electrical responses are clearly showing that some tailoring of the films resistivity was achieved, which will be of major importance to optimized the electrical response according to the major requirements of the targeted application.

Regarding the thermal characteristics, the obtained data are here interpreted assuming a two layer system, the first layer being the $TiAg_x$ film and the second layer the substrate. No interfacial thermal resistance was considered. To guarantee that all the information related to the electronic path of the signal is suppressed, the Modulated IR Radiometry signals were normalized. For normalization semi-infinite opaque body of smooth surface was used. The

resulting normalized amplitude and phase lag signals can be directly compared with the theoretical solutions for a two layer system [47].

Once we are dealing with a two layer system, the method proposed by Fotsing et al.[47] was applied to calculate the thermal parameters needed, namely the thermal diffusion time (τ) and the effusivity ratio (e), where c refers to coating and b to backing or substrate. According to that method, the modulation frequency and the respective phase lag measured at the relative extrema of the inverse calibrated frequency-dependent phase lag signals, in the range of the intermediate modulation frequencies, give direct information on the sample's thermal diffusion time and on the ratio of the thermal effusivities of the two layers (e_c/e_b).

Fig. 8 shows the behavior of the phase lag as a function of the modulation frequency, for a set of $TiAg_x$ samples.

From the thermal diffusion time (τ) and knowing the sample thickness, e.g. from SEM microscopy, one can get immediately the thermal diffusivity (α) of the film from:

$$\tau_c = d_c^2 / \alpha_c \tag{4}$$

The determination of the thermal effusivity of the sample (once e_b is known, usually from the literature) allows one to get the thermal conductivity (k), according to the following simple relations, where ρ represents the density and c the specific heat:

$$e = \sqrt{(k\rho c)} = k/\sqrt{\alpha} \rightarrow k = e\sqrt{\alpha} \tag{5}$$

As in this paper we are mainly interested in knowing the general trends of the prepared samples, and thus only the thermal diffusion time obtained for the $TiAg_x$ thin films will be presented. As one can easily conclude, since the thickness of all samples is quite similar, the thermal diffusivity will follow a trend very close to that of τ.

According to what was already mentioned regarding the structural and morphological characterization as well as the electric resistivity, the thermal analysis also shows the separation between thermal properties of samples with low Ag/Ti ratios (below 0.1) and

higher Ag/Ti ratios. From the amorphization of the Ti phase together with the weak thermal behavior of titanium-silver phases that may be formed, a decrease of phonon transport through the thin film is expected. This becomes clear from Fig. 9, where the thermal diffusion time is quite sensitive to the Ag/Ti ratio.

In fact, one can find two distinct zones with almost constant values of τ, meaning that a structural change took place when going from low to higher Ag/Ti ratios. The same trend was found in the effusivity values, reflecting a significant degradation of the heat conduction mechanisms in the films, and thus an important issue to take into account for the pressure device optimization.

4. CONCLUSIONS

$TiAg_x$ thin films were deposited by DC magnetron sputtering with similar deposition parameters in order to study the influence of silver incorporation into a Ti matrix in the electrical and thermal responses of the produced films.

The results obtained revealed two distinct zones of behaviour. In the first one, identified as Zone I, the samples exhibited a set of features that are very similar to those of the Ti reference film, and where Ag may play the role of an impurity. The lower Ag/Ti atomic ratio (below 3.0×10^{-3}) induces a minimum value of target potential, close to that of the Ti film, and with a growth rate also similar to that of Ti. SEM micrographs confirmed the typical Ti morphology structure, with three-dimensional hexagonal grain features at the surface, and a characteristic columnar-like growth. The resistivity of the samples from this first zone is also similar to that of Ti sample (35 μΩ·cm).

For higher Ag exposed areas (above 1.3 cm^2), the Ag content increased significantly from 6.0×10^{-2} to 3.6×10^{-1}, which gave rise to various changes on the structural and morphological features of the films. XRD patterns evidenced the formation of new phases, coexisting with

the Ti one, which may be indexed to Ti_2Ag or even of TiAg, given the thermodynamic equilibrium suggested by the phase diagram. The existence of these new phases produced samples with smoother surfaces and denser microstructures, with higher grain sizes. As the Ag/Ti atomic ratio increased, a decrease in the resistivity of these samples (from about 70 to 55 μΩ·cm) was obtainbed. $TiAg_x$ thin films from Zone II exhibited also higher values of target potential and lower values of deposition rate.

According with the obtained results, $TiAg_x$ coatings with $0.06 < x < 0.36$ revealed a promising behavior for prosthesis pressure sensors applications, since successful results in electrical and thermal response were obtained coupled with the antibacterial characteristics of the silver and the excellent biocompatibility of the system as a whole.

ACKNOWLEDGEMENTS

This research is partially sponsored by FEDER funds through the program COMPETE – Programa Operacional Factores de Competitividade and by national funds through FCT – Fundação para a Ciência e a Tecnologia, under the projects PTDC/CTM-NAN/112574/2009 and PTDC/SAU-ENB/116850/2010 and Programa Pessoa 2012/2013 Cooperação Portugal/França, Project nº 27306UA. The authors would also like to acknowledge CEMUP for SEM analysis. P. Pedrosa acknowledges FCT for the Ph.D. grant SFRH/BD/70035/2010.

BIBLIOGRAPHY

[1] A.A. Polliack, D.D. Craig, R.C. Sieh, S. Landsberger, D.R. McNeal, Prosthet. Orthot. Int. 26 (2002) 23-24.

[2] N. Ramstrand, K.A. Nilsson, Prosthet. Orthot. Int. 31 (2007) 157-166.

[3] www.crpg.pt/.

[4] N.B. Henrikson, B.J. Hafner, J.R. Dettori, D.C. Norvell, A. Raich, E.D. Brodt, A.C. Skelly, Washington State Health Care Authority, (2011).

[5] C.O. González-Morán, R. González-Ballesteros, E. Suaste-Gómez, 1st. International Conference on Electrical and Electronics Engineering (2004) 473-475.

[6] M.S. Inc., (1999) 1-34.

[7] J.E. McKinney, G.T. Davis, M.G. Broadhurst, J. Appl. Phys. 51 (1980) 1676-1681.

[8] A. Ferrreira, J.G. Rocha, A. Ansón-Casaos, M.T. Martínez, F. Vaz, S. Lanceros-Mendez, Sens. Actuators, A 178 (2012) 10-16.

[9] A. Ferreira, P. Cardoso, D. Klosterman, J.A. Covas, F.W.J. van Hattum, F. Vaz, S. Lanceros-Mendez, Smart Mater. Struct. 21 (2012) 1-9.

[10] J.M. Gonzalez-Dominguez, A. Ansón-Casaos, M.T. Martinez, A. Ferreira, F. Vaz, S. Lanceros-Méndez, J. Intell. Mater. Syst. Struct. 23 (2012) 909-917.

[11] A. Ferreira, P. Pedrosa, S. Lanceros-Mendez, A.V. Machado, F. Vaz, Journal of Optoelectronics and Advanced Materials, 12 (2010) 1581-1589.

[12] A. Ferreira, J. Silva, V. Sencadas, J.L.G. Ribelles, S. Lanceros-Méndez, Macromolecular Materials and Engineering, 295 (2010) 523-528.

[13] J.N. Pereira, P. Vieira, A. Ferreira, A.J. Paleo, J.G. Rocha, S. Lanceros-Méndez, Journal of Polymer Research, 19 (2012) 1-7.

[14] H. Chiriac, M. Urse, F. Rusu, C. Hison, M. Neagu, Sens. Actuators, A 76 (1999) 376-380.

[15] V. Chawla, R. Jayaganthan, A.K. Chawla, R. Chandra, J. Mater. Process. Technol. 209 (2009) 3444-3451.

[16] V. Chawla, R. Jayaganthan, A.K. Chawla, R. Chandra, Mater. Chem. Phys. 111 (2008) 414-418.

[17] K.-H. Liao, K.-L. Ou, H.-C. Cheng, C.-T. Lin, P.-W. Peng, Appl. Surf. Sci. 256 (2010) 3642-3646.

[18] M.A. Fiori, M.M.d.S. Paula, A.M. Bernardin, H.G. Riella, E. Angioletto, Mater. Sci. Eng., C 29 (2009) 1569-1573.

[19] M.F. Santos, C.M. Oliveira, C.T. Tachinski, M.P. Fernandes, C.T. Pich, E. Angioletto, H.G. Riella, M.A. Fiori, Int. J. Miner. Process. 100 (2011) 51-53.

[20] R.X. Wang, X.M. Tao, Y. Wang, G.F. Wang, S.M. Shang, Surf. Coat. Technol. 204 (2010) 1206-1210.

[21] N.P. Barradas, C. Jeynes, Nucl. Instrum. Methods Phys. Res., Sect. B 266 (2008) 1875-1879.

[22] L.J. van der Pauw, Philips Res. Repts 13 (1958) 1-9.

[23] F. Macedo, F. Vaz, A.C. Fernandes, J.L.N. Fotsing, J. Gibkes, J. Pelzl, B.K. Bein, Plasma Processes and Polymers 6 (2009) S592-S598.

[24] F. Macedo, F. Vaz, M. Torrell, R.T. Faria, A. Cavaleiro, N.P. Barradas, E. Alves, K.H. Junge, B.K. Bein, J. Phys. D: Appl. Phys. 45 (2012) 105301.

[25] J. Gibkes, F. Vaz, A.C. Fernandes, P. Carvalho, F. Macedo, R.T. Faria, P. Kijamnajsuk, J. Pelzl, B.K. Bein, J. Phys. D: Appl. Phys. 43 (2010) 395301.

[26] D. Depla, G. Buyle, J. Haemers, R. De Gryse, Surf. Coat. Technol. 200 (2006) 4329-4338.

[27] D. Depla, J. Haemers, R. De Gryse, Thin Solid Films 515 (2006) 468-471.

[28] D. Depla, H. Tomaszewski, G. Buyle, R. De Gryse, Surf. Coat. Technol. 201 (2006) 848-854.

[29] M.A. Lieberman, A.J. Lichtenberg, Wiley, New York, (1994) 81.

[30] S.K. Habib, A. Rizk, I.A. Mousa, Vacuum 49 (1997) 153-160.

[31] N. Bibic, I.H. Wilson, M. Milosavljevic, D. Perusko, Journal of Materials Science 27 (1992) 4945-4948.

[32] K.W. Pierson, J.L. Reeves, T.D. Krueger, C.D. Hawes, C.B. Cooper, Nucl. Instrum. Methods Phys. Res., Sect. B 108 (1996) 290-299.

[33] M. Li, C. Li, F. Wang, W. Zhang, Calphad 29 (2005) 269-275.

[34] www.webelements.com/.

[35] J.F. Pierson, D. Horwat, Scripta Mater. 58 (2008) 568-570.

[36] J.G. Han, H.S. Myung, H.M. Lee, L.R. Shaginyan, Surf. Coat. Technol. 174-175 (2003) 738-743.

[37] X. Wang, F. Prokert, H. Reuther, M.F. Maitz, F. Zhang, Surf. Coat. Technol. 185 (2004) 12-17.

[38] C. Guo, J. Chen, J. Zhou, J. Zhao, L. Wang, Y. Yu, H. Zhou, Appl. Surf. Sci. 257 (2011) 10692-10698.

[39] J.-B. Han, Y.-B. Han, D.-J. Chen, S. Ding, Q.-Q. Wang, Mater. Lett. 60 (2006) 467-469.

[40] A. Ewald, S.K. Gluckermann, R. Thull, U. Gbureck, Biomedical Engineering Online 5 (2006) 1-10.

[41] H. Cao, X. Liu, F. Meng, P.K. Chu, Biomaterials 32 (2011) 693-705.

[42] R. Catrin, D. Horwat, J.F. Pierson, S. Migot, Y. Hu, F. Mücklich, Appl. Surf. Sci. 257 (2011) 5223-5229.

[43] T. Suzuki, Y. Abe, M. Kawamura, K. Sasaki, T. Shouzu, K. Kawamata, Vacuum 66 (2002) 501-504.

[44] S. Nagarjuna, K. Balasubramanian, D.S. Sarma, Mater. Sci. Eng., A 225 (1997) 118-124.

[45] E. Gratz, Encyclopedia of Materials: Science and Technology (Second Edition), (2001) 4152-4158.

[46] M.E. Day, M. Delfino, J.A. Fair, W. Tsai, Thin Solid Films 254 (1995) 285-290.

[47] J.L. Nzodoum Fotsing, J. Gibkes, J. Pelzl, B.K. Bein, J. Appl. Phys. 98 (2005) 063522.

Figure captions

Fig. 1. Discharge characteristics of $TiAg_x$ thin films: evolution of the target potential **(a)** and the deposition rate **(b)** with increasing Ag area exposed in the target.

Fig. 2. Evolution of $TiAg_x$ thin films chemical composition as a function of the Ag exposed area in the Ti target

Fig. 3. XRD diffraction patterns for different Ag contents in $TiAg_x$ prepared coatings; (a) full scale diffractograms and (b) 37,4º - 38,8º magnification

Fig. 4. Experimental and fitted reflectance for samples with different Ag/Ti atomic ratios, compared with Ti and Ag reference thin films.

Fig. 5. Experimental SEM Plan view ($a_1 - f_1$) and cross-section ($a_2 - f_2$) micrographs of the reference thin films: a) Ti; f) Ag and for samples with different Ag/Ti atomic ratios: b) 0.0022; c) 0.0641; d) 0.1262; e) 0.2271. All the images were obtained with the same magnitude resolution: 50 000 x.

Fig. 6. Electrical resistivity, measured at room temperature, as a function of Ag/Ti atomic ratio.

Fig. 7. Grain size evolution of Ti and TiAg/Ag phases with increasing Ag/Ti atomic ratio.

Fig. 8. Inverse normalized modulated IR phase lag signals, measured as a function of the heating modulation frequency for a set of TiAg thin films. Solid lines correspond to theoretical fits, according to the two layer model.

Fig. 9. Evolution of the thin films' thermal diffusion time τc with the Ag /Ti ratio.

Figure 1

a)

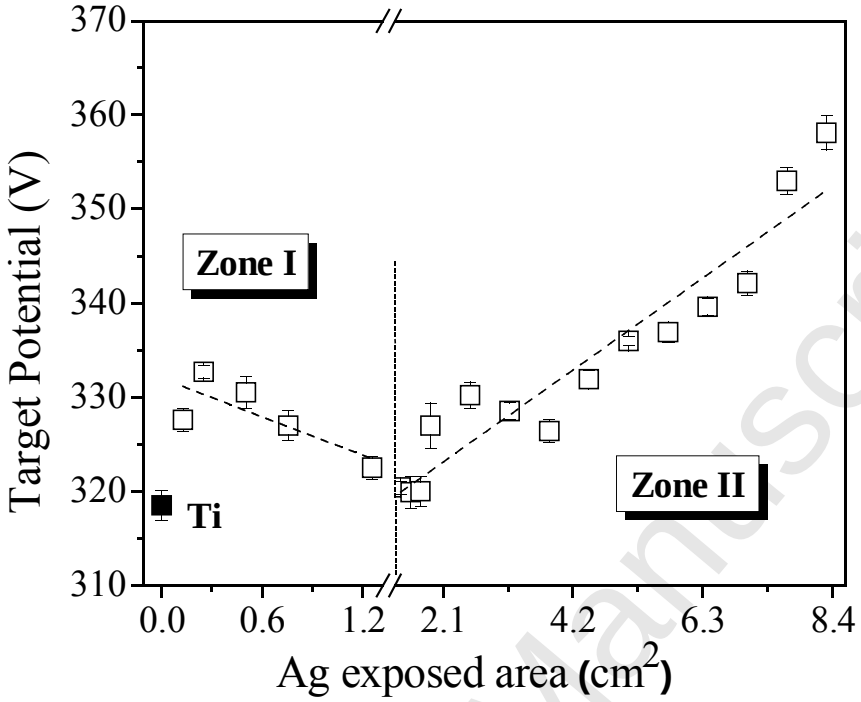

b)

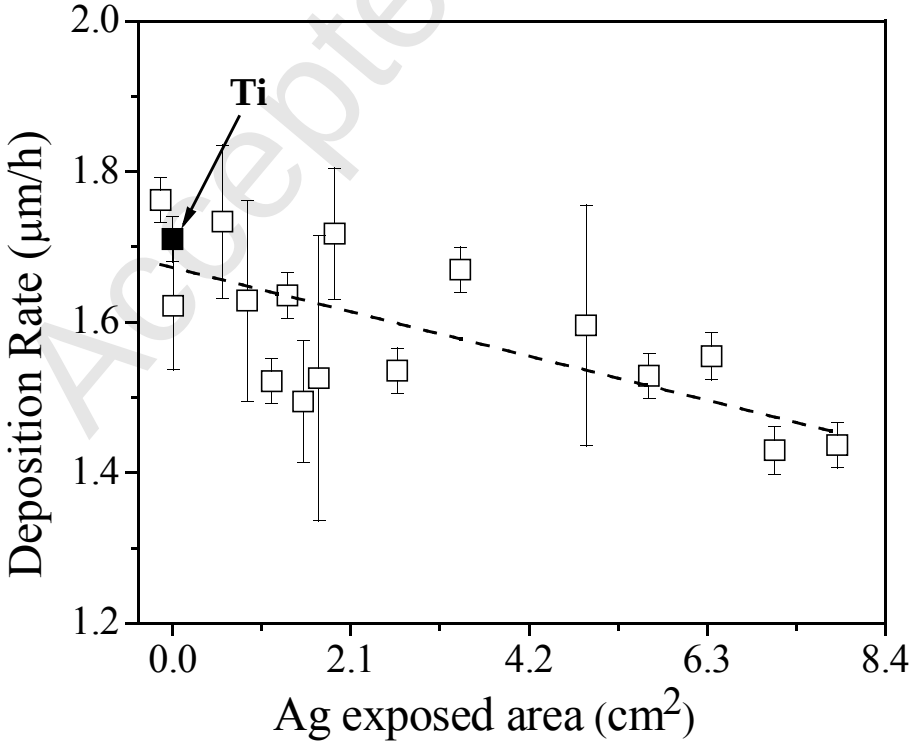

Figure 2

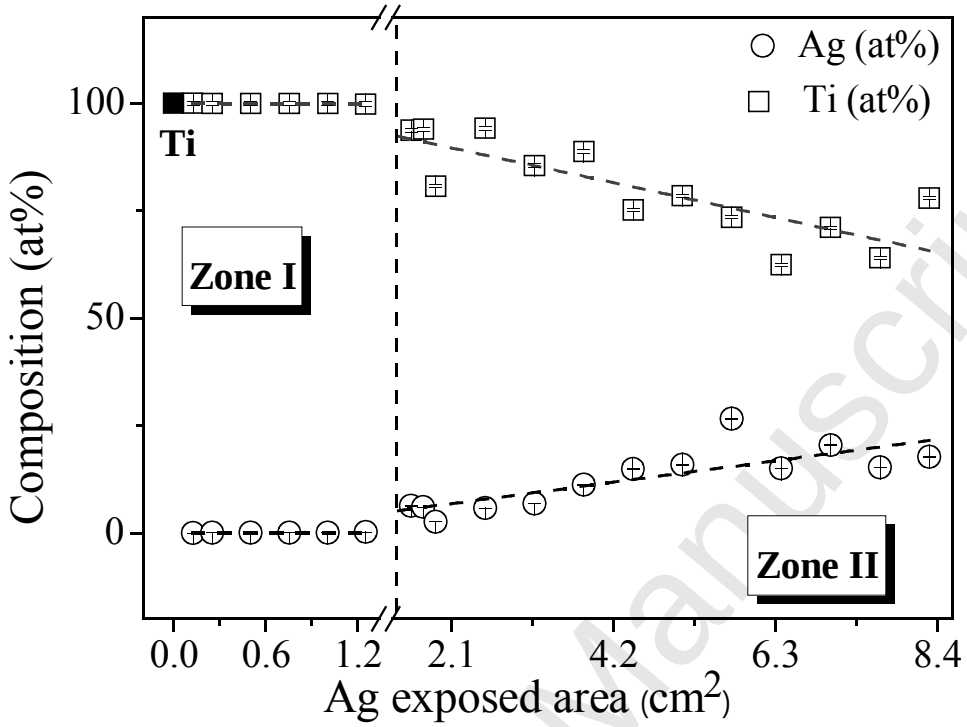

Figure 3

a)

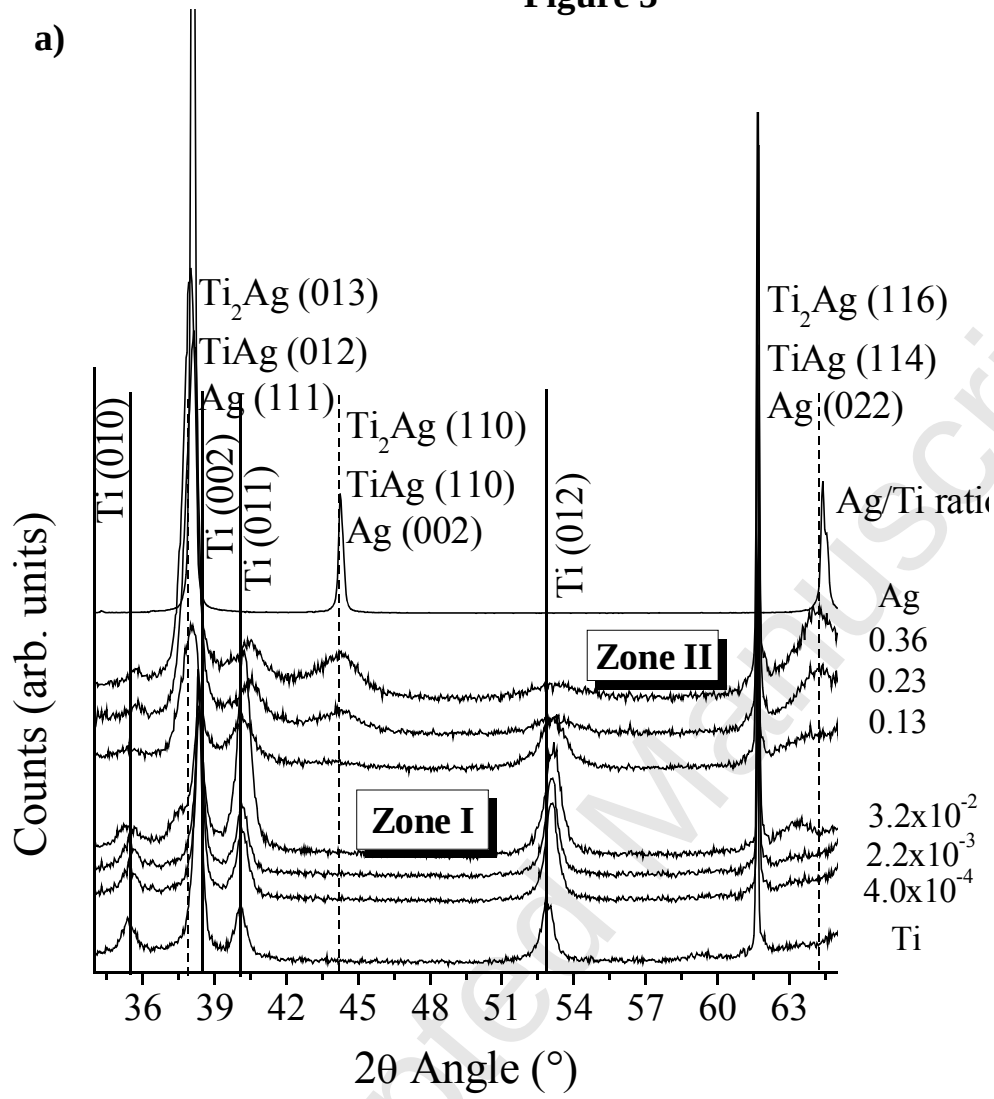

b)

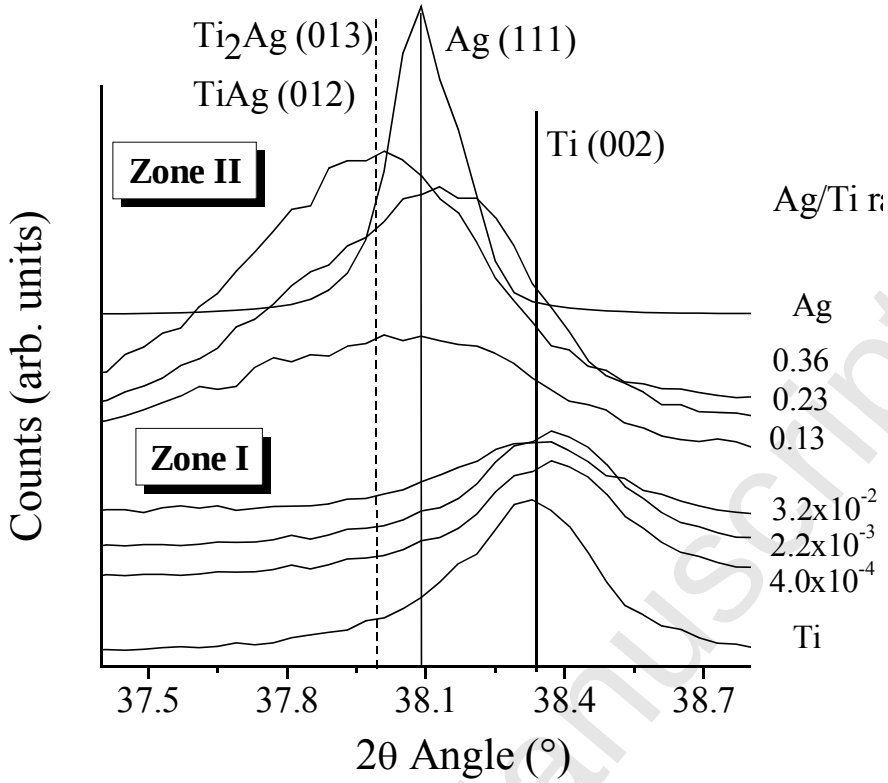

Figure 4

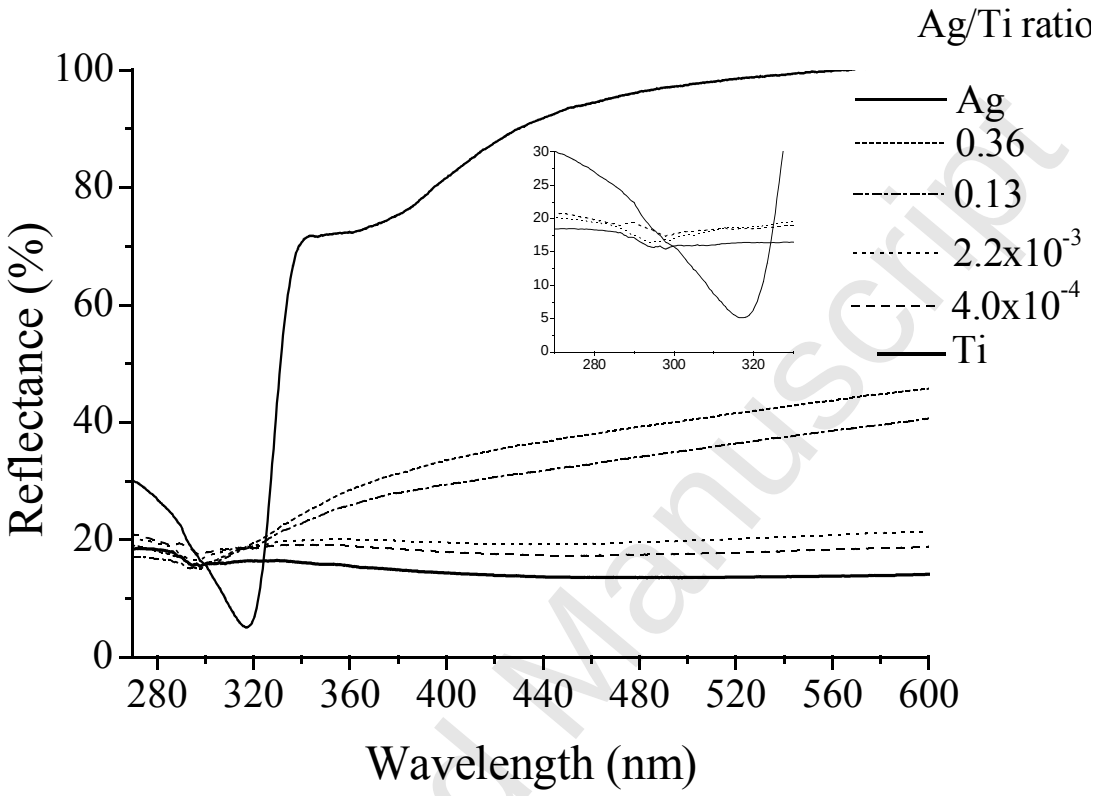

Figure 5

Zone I

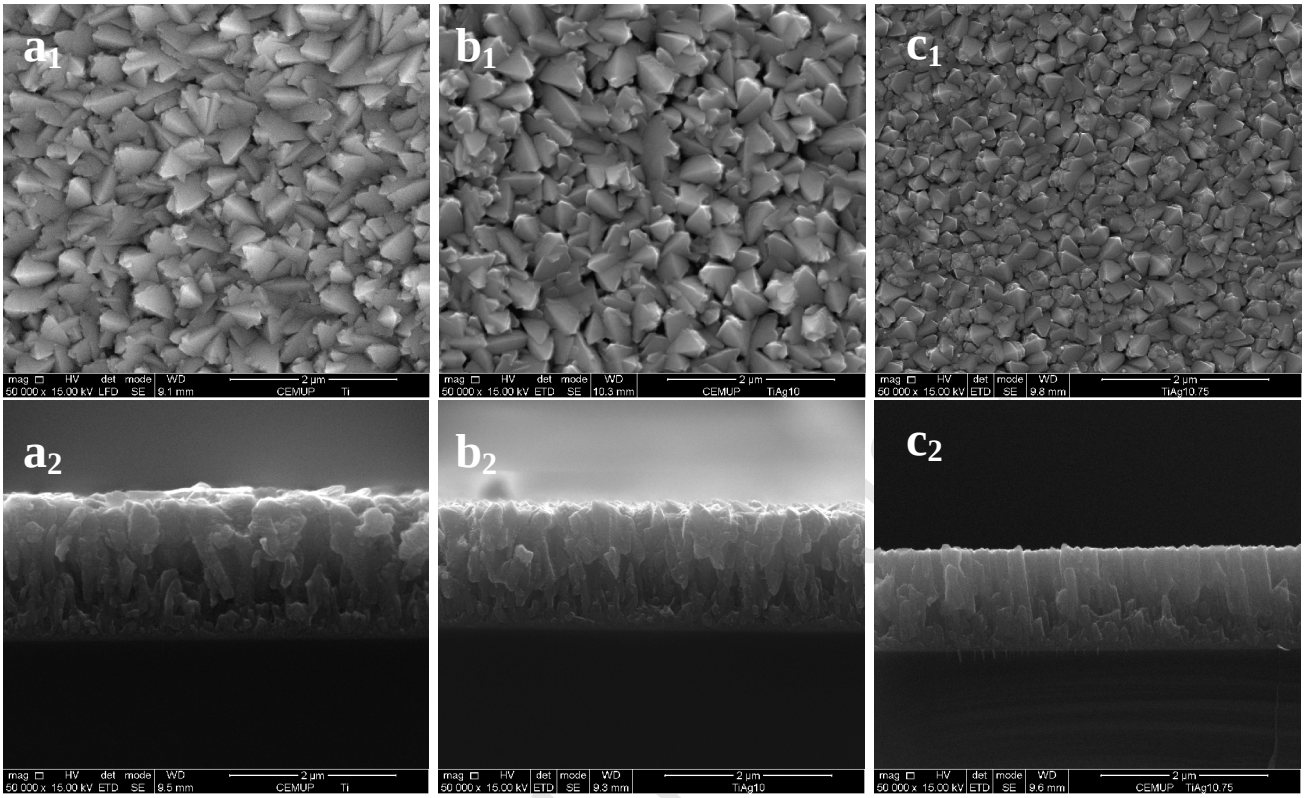

Zone II

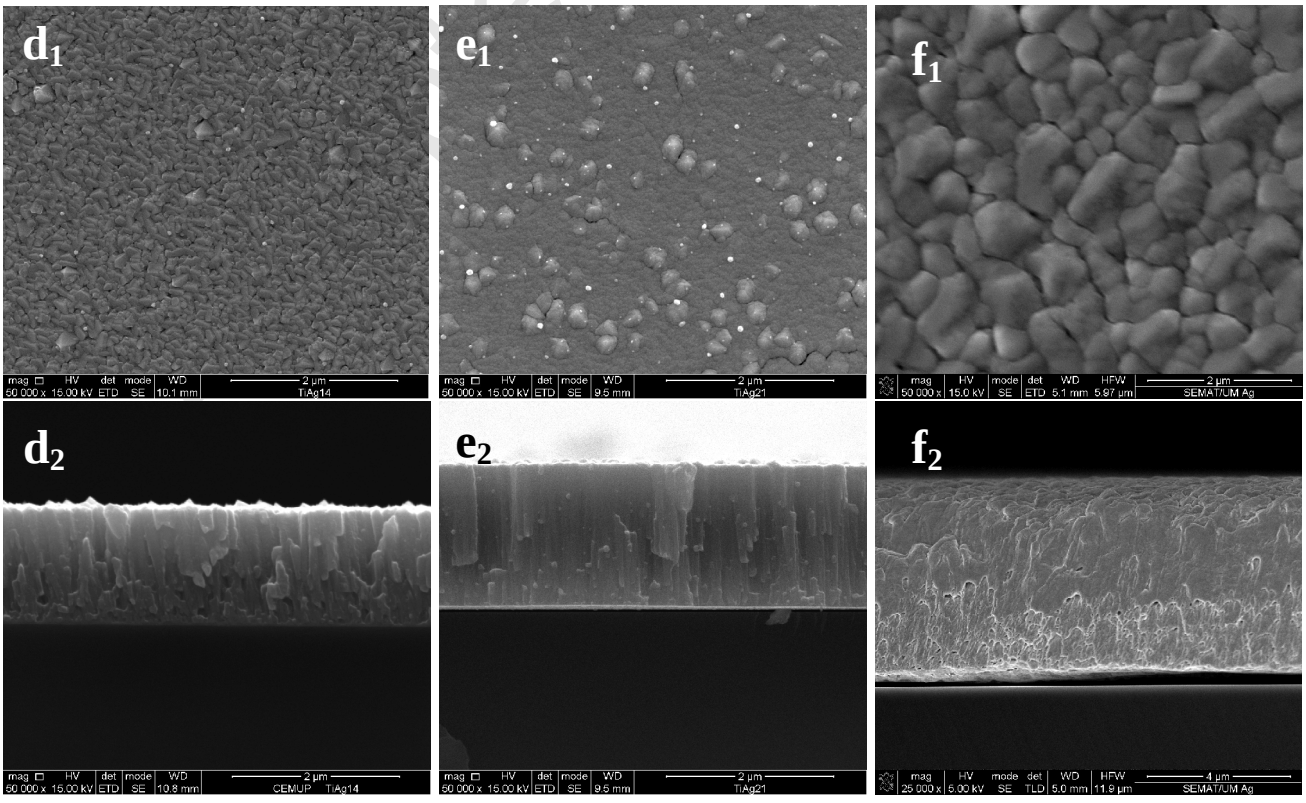

Figure 6

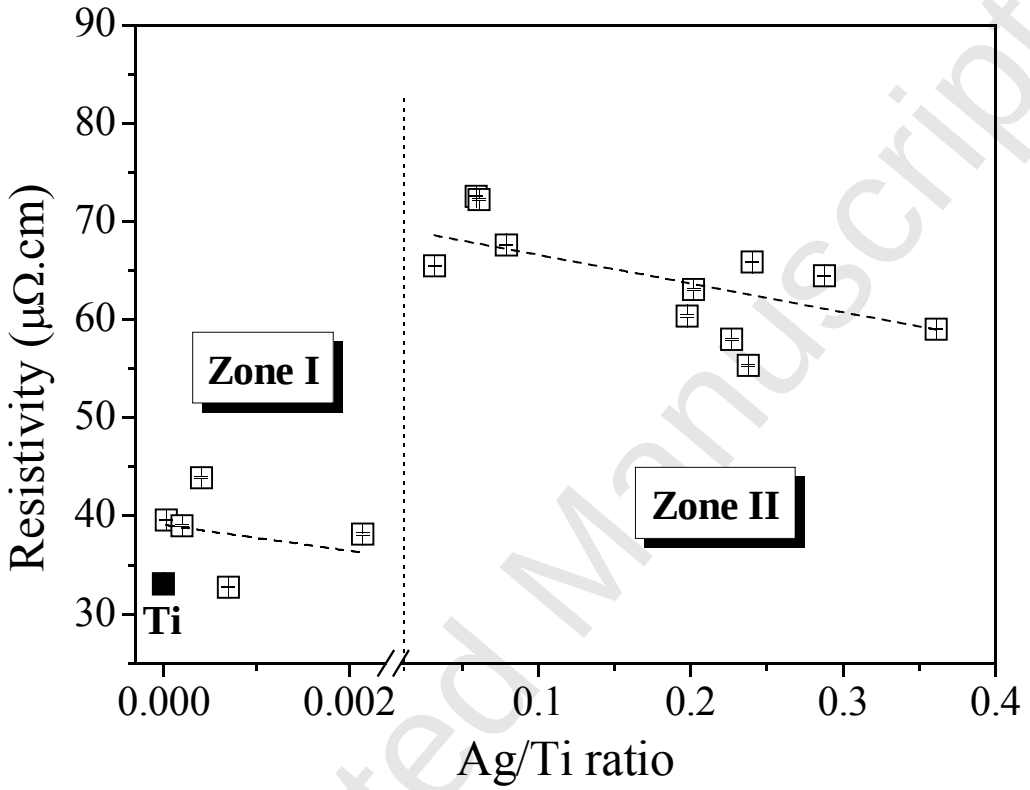

Figure 7

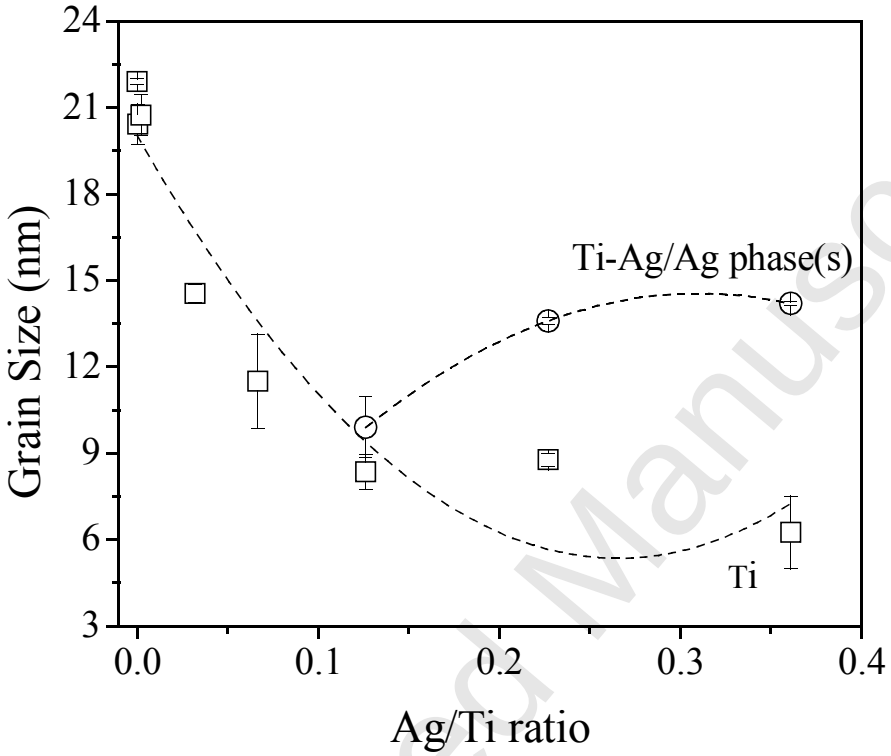

Figure 8

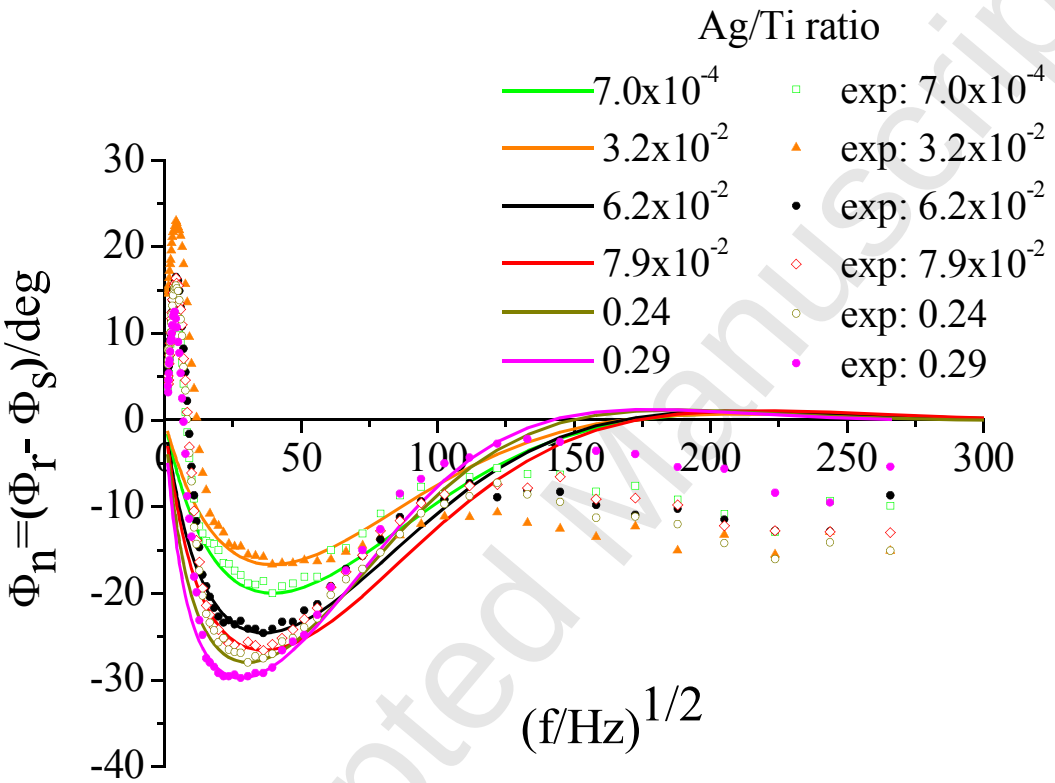

Figure 9